Supplementary information

Porous boron nitride for combined CO$_2$ capture and photoreduction

Ravi Shankar[a], Michael Sachs[b], Laia Francàs[b], Daphné Lubert-Perquel[c], Gwilherm Kerherve[d], Anna Regoutz[d], and Camille Petit[a*]

[a]Barrer Centre, Department of Chemical Engineering, Imperial College London, South Kensington Campus, Exhibition Road, London SW7 2AZ, United Kingdom

[b]Department of Chemistry, Imperial College London, South Kensington Campus, Exhibition Road, London SW7 2AZ, United Kingdom

[c]London Centre for Nanotechnology and Department of Materials, Imperial College London, South Kensington Campus, Prince's Consort Road, London SW7 2BP, United Kingdom

[d]Department of Materials, Imperial College London, South Kensington Campus, Prince's Consort Road, London SW7 2BP, United Kingdom

Corresponding author:

E-mail: camille.petit@imperial.ac.uk; Phone: +44 (0)20 7594 3182 (C. Petit)

Supplementary Table 1. Textural parameters derived from N_2 sorption isotherms obtained at -196 °C for the materials investigated in this study.

Sample	S_{BET} $(m^2\ g^{-1})$	V_{tot} $(cm^3\ g^{-1})$	V_{micro} $(cm^3\ g^{-1})$	V_{micro}/V_{tot} (%)
Porous BN *Before CO$_2$ reaction*	1585	1.10	0.66	60.0
Porous BN *After CO$_2$ reaction (CO$_2$/H$_2$)*	1196	1.01	0.44	43.6
Porous BN *After CO$_2$ reaction (CO$_2$/H$_2$O)*	1190	0.94	0.49	52.1
***h*-BN**	3	0.006	0.001	16.7
P25	48	0.112	0.016	14.3
g-C$_3$N$_4$	32	0.164	0.020	12.1

a
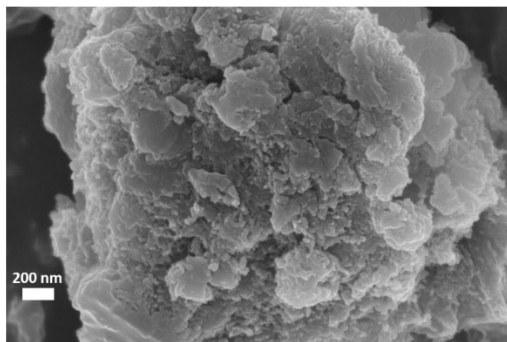
b
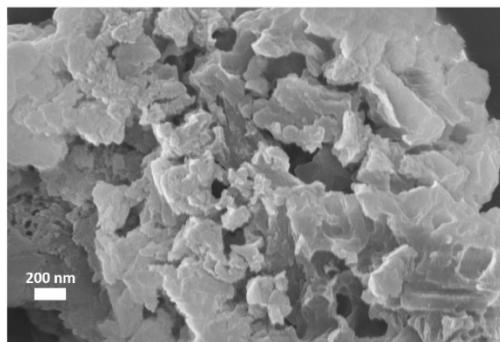
Supplementary Figure 1 I SEM image of the porous BN catalyst taken (**a**) before and (**b**) after the CO_2 photoreduction reaction.
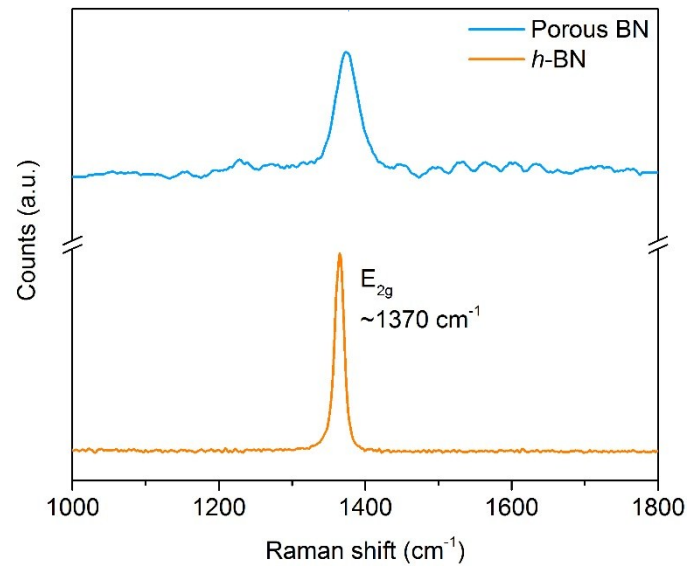
Supplementary Figure 2 I Raman spectra for porous BN compared to *h*-BN.
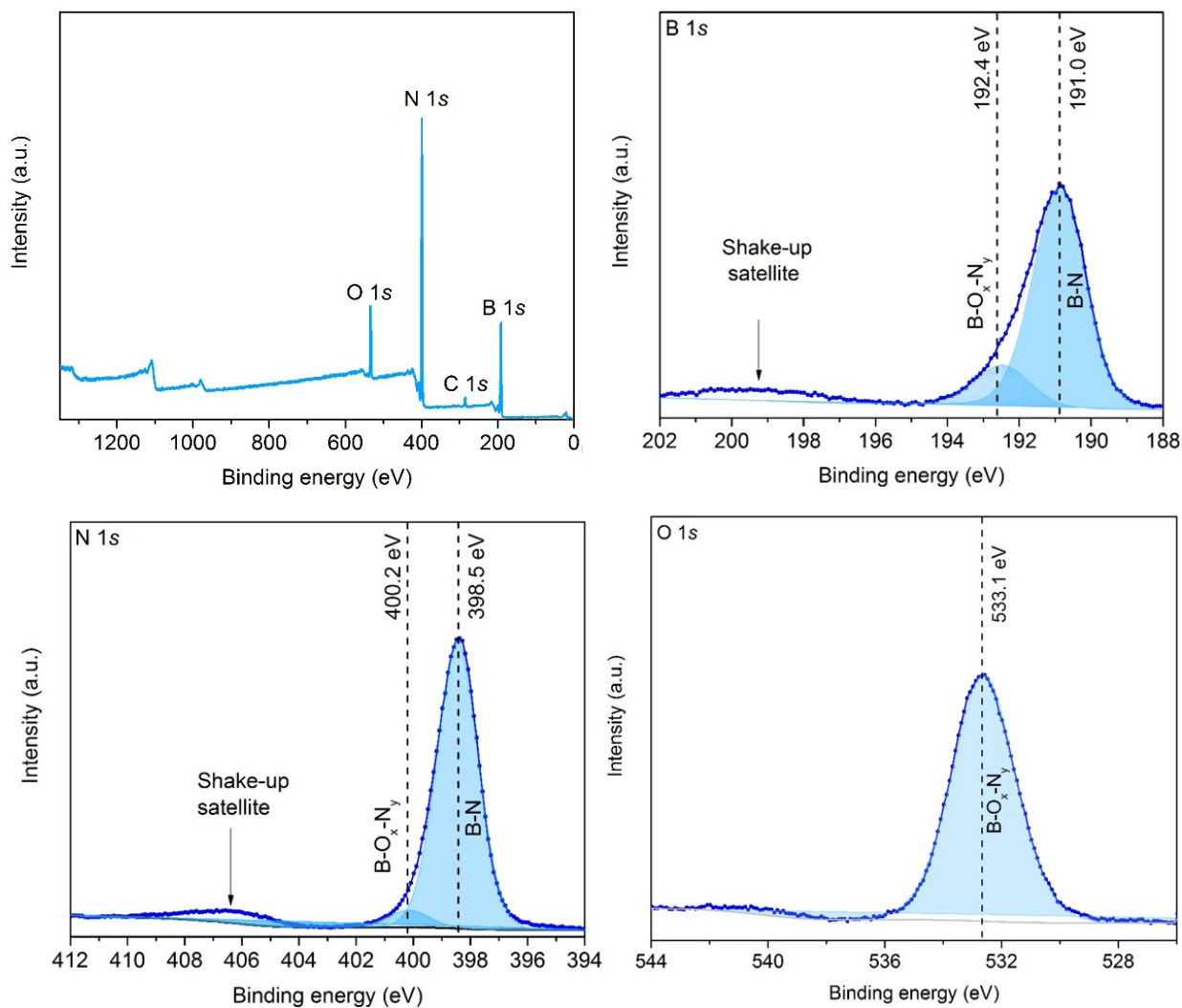
Supplementary Figure 3 I Chemical composition and states in porous BN before CO₂ photoreduction. Survey spectrum and high resolution XPS core level spectra for B 1*s*, N 1*s* and O 1*s* with the key characteristic peaks and corresponding binding energies highlighted.
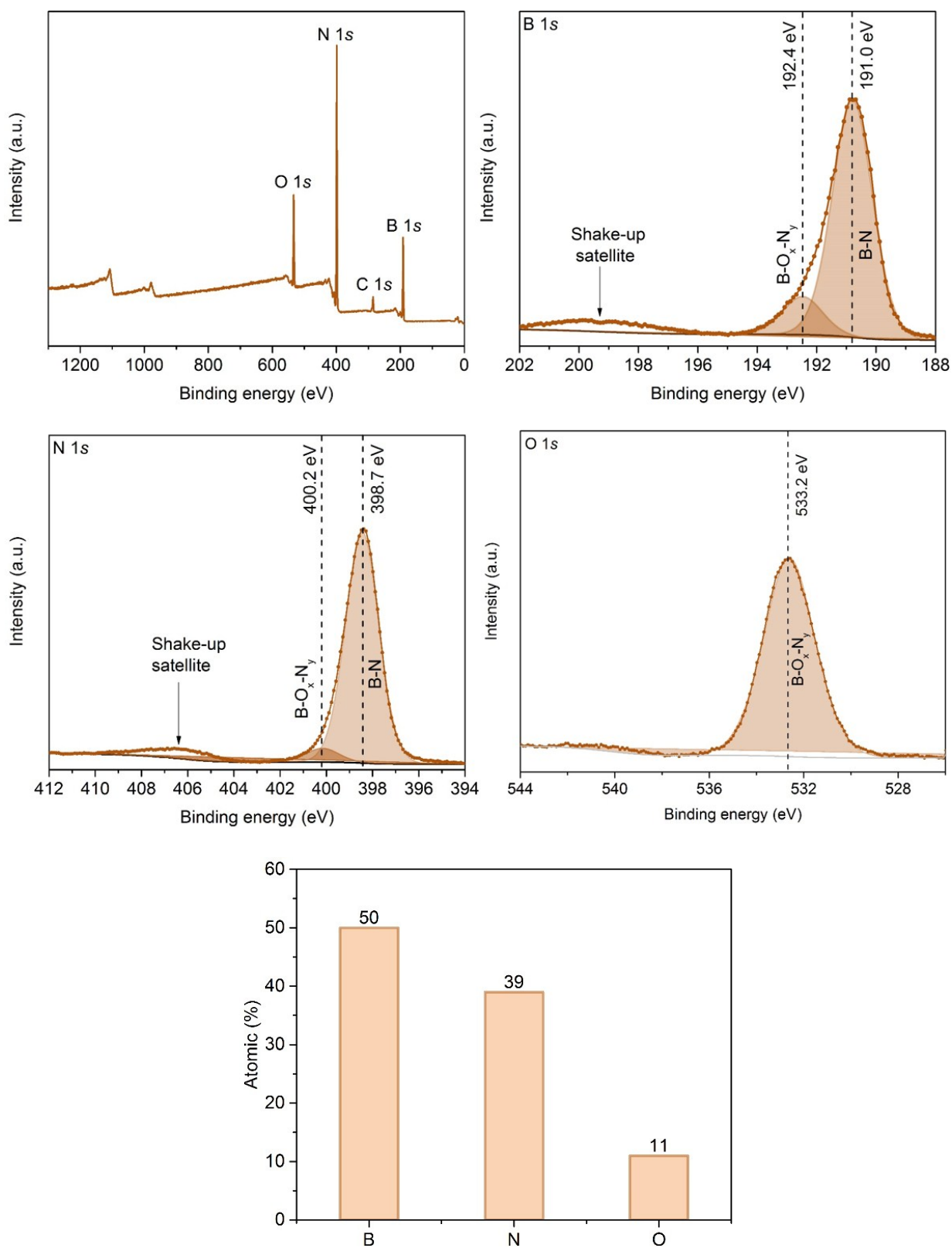
Supplementary Figure 4 I Chemical composition and states of porous BN after CO$_2$ photoreduction. Survey spectrum and high resolution XPS core level spectra for B 1*s*, N 1*s* and O 1*s* with the key characteristic peaks and corresponding binding energies highlighted.
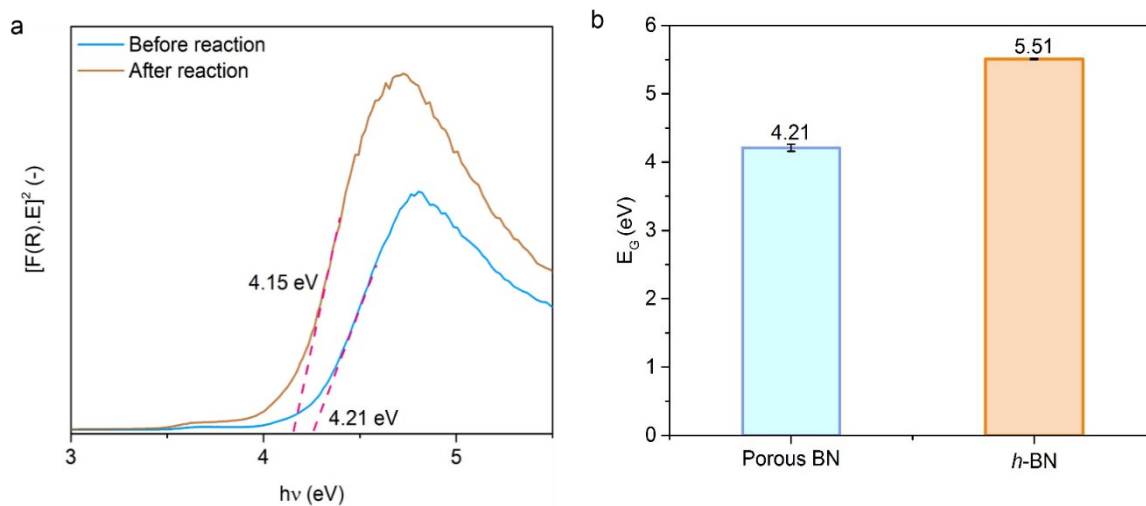
Supplementary Figure 5 I (**a**) Tauc plot of the Kubelka-Munk function versus photon energy to determine the optical band gap of the porous BN material before and after photocatalytic CO_2 reduction reaction, (**b**) Optical band gaps of porous BN compared to h-BN.
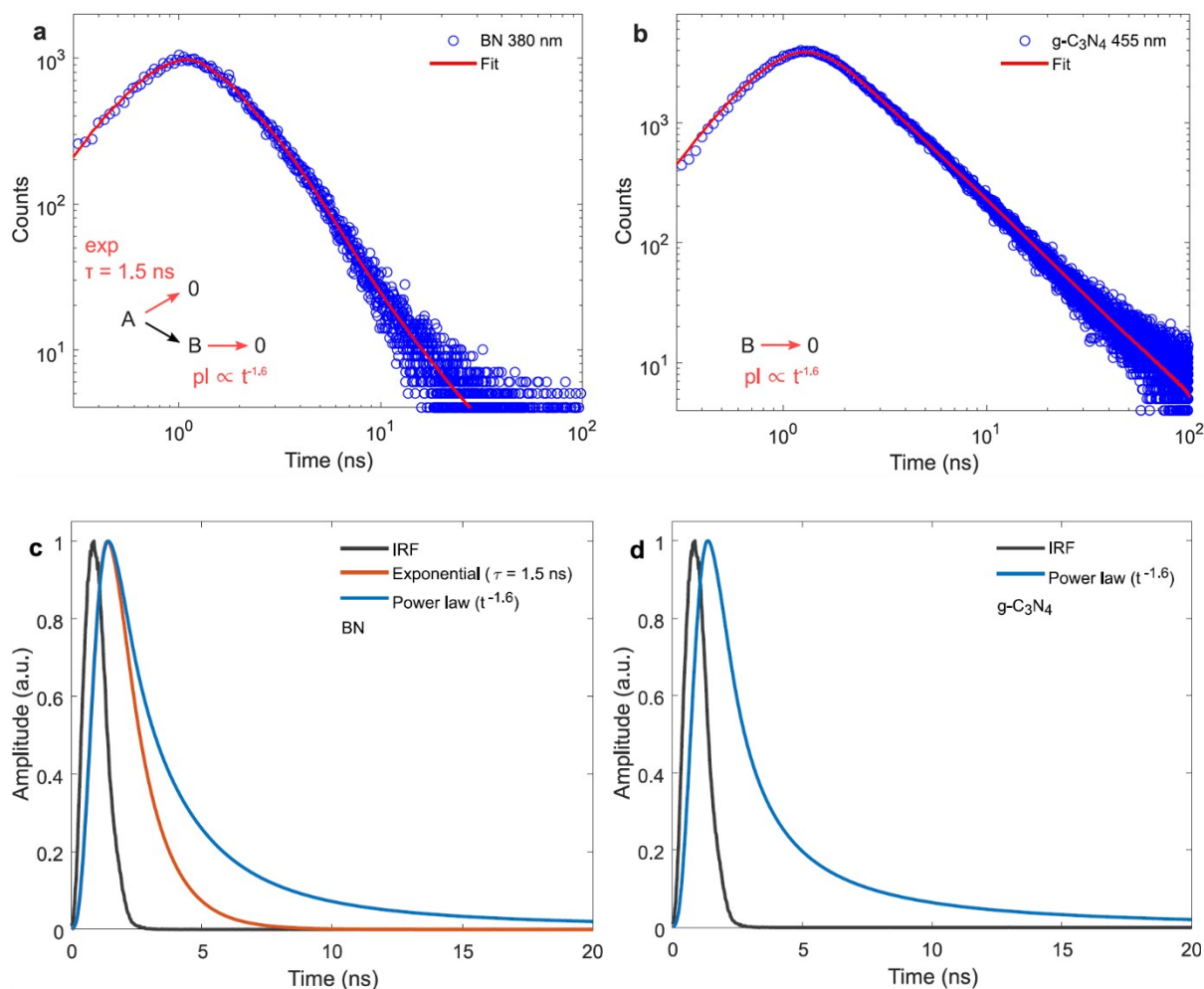
Supplementary Figure 6 | Exemplary time-resolved emission (TRES) kinetics and global fits for **(a)** BN probed at 380 nm and **(b)** g-C$_3$N$_4$ probed at 455 nm. The inset illustrates the model for the respective global fit with red arrows indicating the radiative transitions that give rise to the measured photoluminescence signal and 0 denotes the ground state. For g-C$_3$N$_4$, the TRES dataset is well-represented by a single component (B) that decays with a power law decay $\propto$ t$^{-1.6}$, assigned to shallowly trapped charges. For BN, two components are required for a satisfactory fit: an exponentially decaying component (A) with a time constant τ = 1.5 ns plus a second component (B) decaying with a power law decay $\propto$ t$^{-1.6}$, assigned to excitons and shallowly trapped charges respectively. The spectra obtained for the individual components from this global fit procedure are presented in Figure 2e and 2f in the main text. The corresponding fitted decay kinetics for each component are shown here for **(c)** BN and **(d)** g-C$_3$N$_4$. IRF denotes the instrument response function.

We note that no pronounced spectral evolution was previously observed for g-C$_3$N$_4$ even upon excitation at longer wavelengths, suggesting that the longer exciton lifetime observed for BN is not due to the smaller excess energy upon 282 nm excitation as compared to the smaller band gap of g-C$_3$N$_4$.[1]
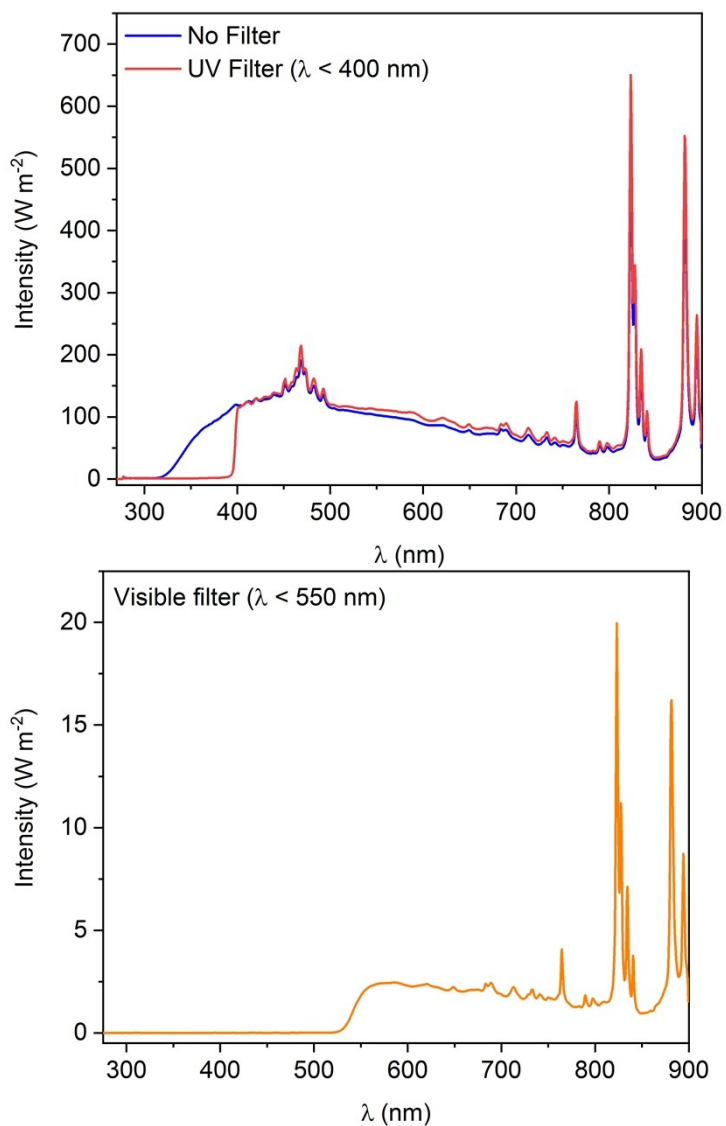
Supplementary Figure 7 I 300 W Xe arc lamp with water filter emission spectra with and without the UV filter (λ < 400 nm) (LOT Quantum Design) and visible light filter (λ < 550 nm) (Thor Labs). Distance from lamp to catalyst surface is 9.5 cm.

Supplementary Table 2. Summary of the CO evolution rates for porous BN for all of the photocatalytic CO_2 reduction reactions conducted.

Reaction	CO evolution rate (UV-Vis) (μmol g^{-1} h^{-1})
UV-Vis (CO_2/H_2)	1.17
UV-Vis (CO_2/H_2O)	0.80
Visible (CO_2/H_2) (λ > 400 nm)	0.20
Visible (CO_2/H_2) (λ > 550 nm)	n.d
Blank run (no photocatalyst)	n.d
Dark run	n.d
N_2/H_2 run	n.d
$^{13}CO_2$ isotopic test	1.10

n.d – none detected
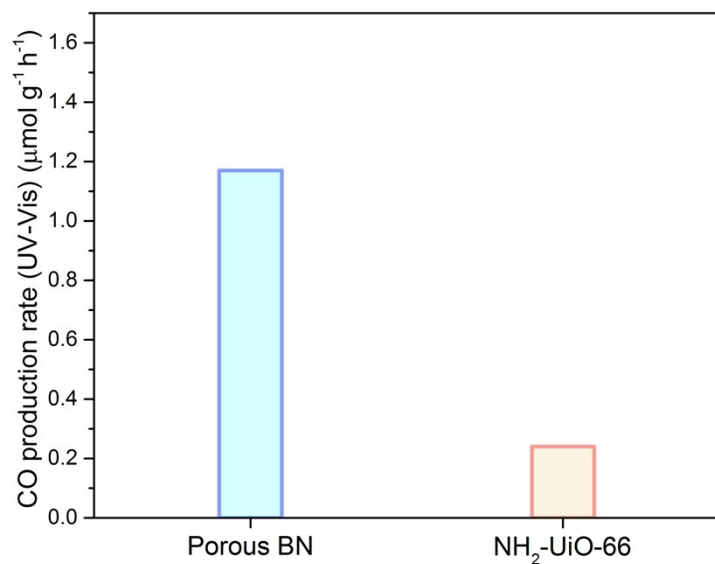
Supplementary Figure 8 I Comparison of specific CO production rate from porous BN with the porous NH_2-UiO-66 MOF as synthesised by Crake et al. (*Small* 2019, 15, 1805473, which exhibits a specific surface area of 871 m^2 g^{-1} and a band gap of 2.82 eV.[2]
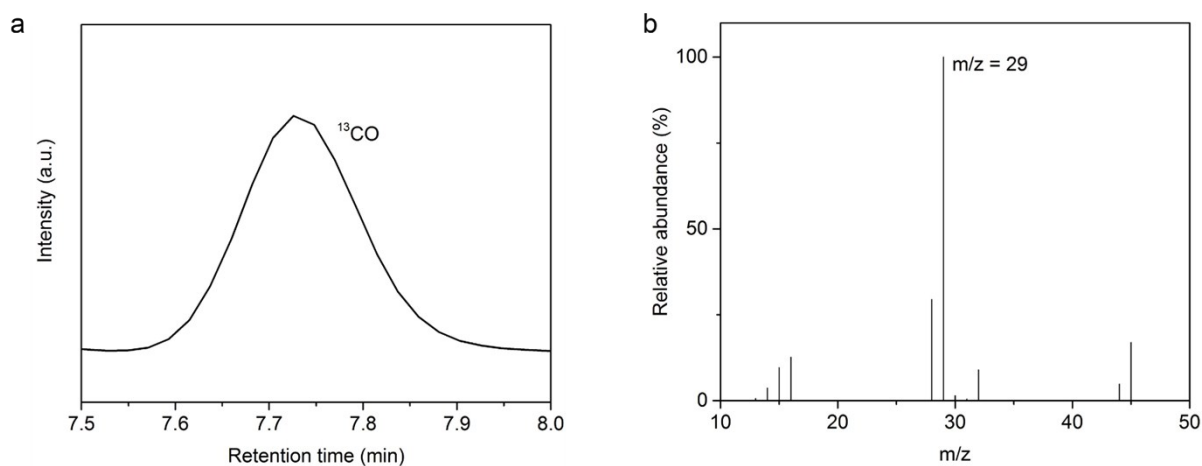
Supplementary Figure 9 I (**a**) Gas chromatogram illustrating the ^{13}CO peak observed with the photocatalytic $^{13}CO_2$ reduction system, (**b**) Mass spectra for the photocatalytic $^{13}CO_2$ reduction system with the peak corresponding to ^{13}CO (m/z = 29) indicated. All of the peak intensities have been scaled relative to the intensity of the m/z = 29 peak.
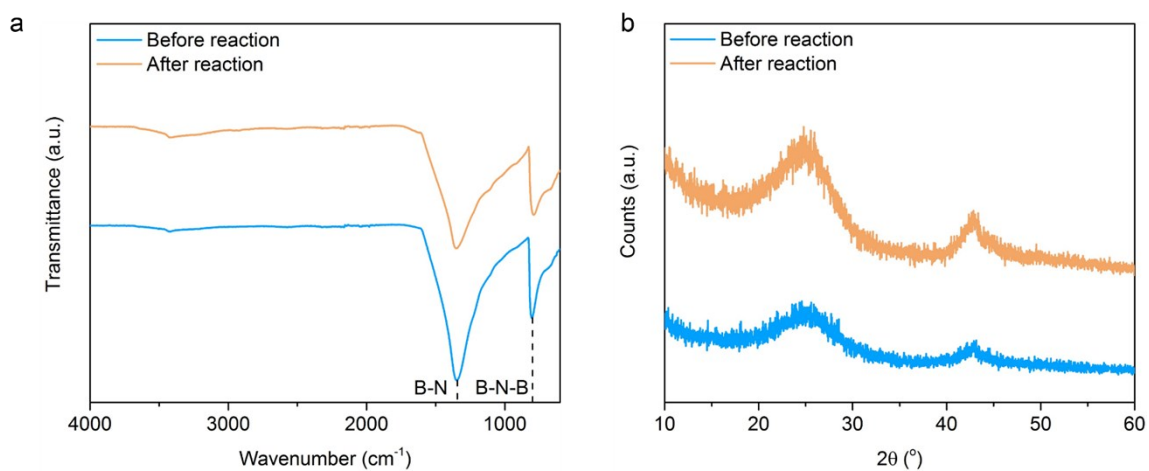
Supplementary Figure 10 I (a) Comparison of the FT-IR spectra of the porous BN before and after the CO_2 photoreduction reaction, with key characteristic bands highlighted, **(b)** Comparison of the XRD patterns of the porous BN before and after the CO_2 photoreduction reaction.
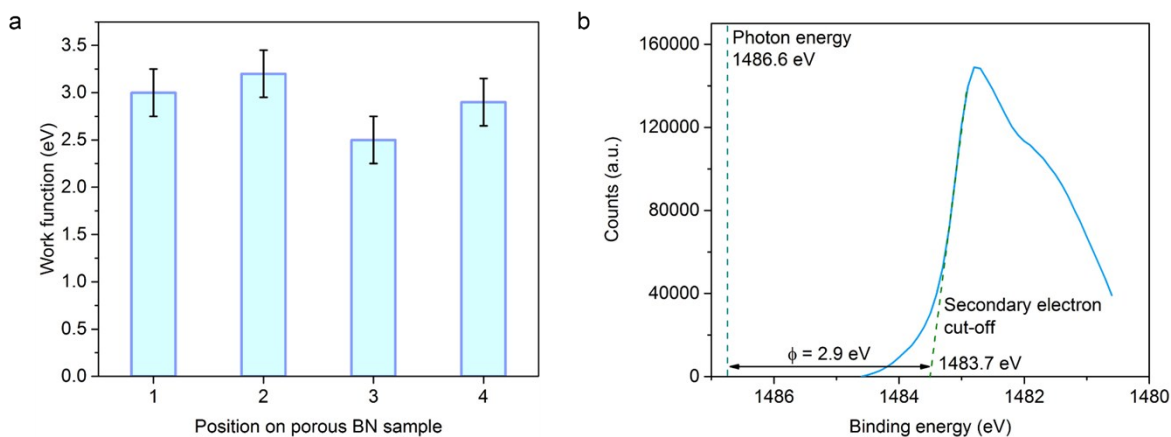
Supplementary Figure 11 I (**a**) Work function measurements at four opposite locations on the porous BN sample to account for potential variations across the surface – only minimal variation was observed, (**b**) Secondary electron cut-off for porous BN measured through photoelectron spectroscopy. The energy associated to the monochromatic photon source in the XPS instrument is indicated, at which point the electrons have zero kinetic energy. The secondary electron-cut off denotes the threshold value at which point the electrons have sufficient kinetic energy to overcome the work function of the material and be detected by the spectrometer. Extrapolation of the secondary electron cut-off yields the work function of the material.

Error propagation analysis in the band structure of porous BN

The average work function (Φ) measured through photoelectron spectroscopy was:

$$\Phi = 2.90 \text{ eV} \pm 0.30 \text{ eV}$$

The position of the Fermi level (E_F) on the absolute energy scale is given by:

$$E_F = E_{VAC} + \Phi$$

For a sum of two terms, the total error can be approximated as the sum of the individual errors associated to each term, hence:

$$\delta E_F \approx \delta E_{VAC} + \delta\Phi,$$

where δX denotes the error in quantity X. So, it follows:

$$\delta E_F \approx (0 + 0.30) \text{ eV} \approx 0.30 \text{ eV, and}$$
$$E_F = 2.90 \pm 0.30 \text{ eV}$$

The position of the valence band (VB) on the absolute energy scale can then be calculated through knowledge of the valence band offset measured through XPS:

$$E_{VB} = E_F + E_{VB-EF}$$
$$\delta E_{VB} \approx \delta E_F + \delta E_{VB-EF}$$

$$\delta E_{VB} \approx (0.30 + 0.02) \text{ eV} \approx 0.32 \text{ eV, so}$$
$$E_{VB} = 2.90 + 3.05 = 5.95 \text{ eV} \pm 0.32 \text{ eV}$$

The position of the conduction band (CB) on the absolute energy scale can then be calculated through knowledge of the band gap (E_G):

$$E_{CB} = E_{VB} - E_G$$
$$\delta E_{CB} \approx \delta E_{VB} + \delta E_G$$

$$\delta E_{CB} \approx (0.32 + 0.05) \text{ eV} \approx 0.37 \text{ eV, so}$$

$$E_{CB} = 5.95 - 4.21 = 1.14 \text{ eV} \pm 0.37 \text{ eV}$$

References

1.   R. Godin; Y. Wang; M. A. Zwijnenburg; J. Tang; J. R. Durrant. *Journal of the American Chemical Society,* 2017, **139**, 5216-5224.

2.   A. Crake; K. C. Christoforidis; A. Gregg; B. Moss; A. Kafizas; C. Petit. *Small,* 2019, **15**, 1805473.